Journal of Controlled Release 350 (2022) 514–524

Contents lists available at ScienceDirect

Journal of Controlled Release

journal homepage: www.elsevier.com/locate/jconrel

Impact of doubling peptide length on *in vivo* hydrogel stability and sustained drug release☆

Julie Heremans [a], Lucie Chevillard [b], Morgane Mannes [a], Jessica Mangialetto [c], Kaat Leroy [d], Jacinta F. White [e], Arthur Lamouroux [a], Mathieu Vinken [d], James Gardiner [e], Bruno Van Mele [c], Niko Van den Brande [c], Richard Hoogenboom [f], Annemieke Madder [g], Vicky Caveliers [h], Bruno Mégarbane [b,*], Sophie Hernot [h,*], Steven Ballet [a,*], Charlotte Martin [a,*]

[a] *Research Group of Organic Chemistry, Vrije Universiteit Brussel, Pleinlaan 2, B-1050 Brussels, Belgium*
[b] *INSERM, UMR-S 1144, Université de Paris, F-75006 Paris, France*
[c] *Physical Chemistry and Polymer Science, Vrije Universiteit Brussel, Pleinlaan 2, B-1050 Brussels, Belgium*
[d] *Department of Pharmaceutical and Pharmacological Sciences, Faculty of Medicine and Pharmacy, Vrije Universiteit Brussel, Laarbeeklaan B-103, 1090 Brussels, Belgium*
[e] *CSIRO Manufacturing, Bayview Avenue, Clayton, VIC 3169, Australia*
[f] *Supramolecular Chemistry Group, Department of Organic and Macromolecular Chemistry, Ghent University, Krijgslaan 281, 9000 Ghent, Belgium*
[g] *Organic and Biomimetic Chemistry Research Group, Ghent University, Krijgslaan 281, 9000 Ghent, Belgium*
[h] *In Vivo Cellular and Molecular Imaging, Vrije Universiteit Brussel, Laarbeeklaan 103, 1090 Brussels, Belgium*

ARTICLE INFO

Keywords:
Peptide-based hydrogels
In vivo imaging
Subcutaneous administration
Sustained drug release
Mechanical properties
Antinociceptive efficacy

ABSTRACT

Peptide-based hydrogels represent promising systems for the sustained release of different types of drugs, ranging from small molecules to biologicals. Aiming at subcutaneous injection, which is a desirable parenteral administration route, especially for biologicals, we herein focus on physically crosslinked systems possessing thixotropic behaviour. The purpose of this study was to evaluate the *in vitro* and *in vivo* properties of hydrogels based on the amphipathic hexapeptide H-FQFQFK-NH_2, which served as the lead sequence. Upon doubling the length of this peptide, the dodecapeptide H-FQFQFKFQFQFK-NH_2 gave a significant improvement in terms of *in vivo* stability of the hydrogel post-injection, as monitored by nuclear SPECT/CT imaging. This increased hydrogel stability also led to a more prolonged *in vivo* release of encapsulated peptide cargoes. Even though no direct link with the mechanical properties of the hydrogels before injection could be made, an important effect of the subcutaneous medium was noticed on the rheological properties of the hydrogels in post *in vivo* injection measurements. The results were validated *in vivo* for a therapeutically relevant analgesic peptide using the hot-plate test as an acute pain model. It was confirmed that elongation of the hydrogelator sequence induced more extended antinociceptive effects. Altogether, this simple structural modification of the hydrogelating peptide could provide a basis for reaching longer durations of action upon use of these soft biomaterials.

1. Introduction

Subcutaneous administration is commonly used to deliver drugs under the skin, more precisely into the subcutis [1,2]. This way of administration is desirable when systemic drug absorption is targeted, allowing to circumvent the gastrointestinal tract and first-pass metabolism, in order to increase bioavailability [2–4]. This is especially suitable for biologicals that exhibit poor oral bioavailability [4–6]. Generally, subcutaneous injection is the preferred parenteral administration route due to intrinsic advantages such as high effectiveness and safety, relative low-cost and high patient compliance [1,6–8]. Therefore, subcutaneous drug delivery systems represent an attractive approach for the treatment of chronic diseases, requiring frequent drug administrations [9]. Consequently, substantial efforts have been dedicated to improve subcutaneous formulations, aiming to prolong drug exposure and increase patient compliance by reducing the number of injections

☆ This work is dedicated to the career and lifetime achievements of Honorary Rector Prof. Dr. Caroline Pauwels.

* Corresponding authors.
E-mail addresses: steven.ballet@vub.be (S. Ballet), charlotte.martin@vub.be (C. Martin).

https://doi.org/10.1016/j.jconrel.2022.08.027
Received 14 December 2021; Received in revised form 10 August 2022; Accepted 13 August 2022
Available online 1 September 2022

[4,7,10]. Hydrogels, introduced in the 1960s, are an example of a promising sustained drug delivery formulation. They can be defined as a three-dimensional network retaining large amounts of water [11–14]. More specifically, this functional biomaterial can be formed from low-molecular-weight building blocks that can assemble into nanofibers through non-covalent interactions, involving hydrogen bonds, π-π stacking, hydrophobic effects and electrostatic interactions [13,15]. Among these building blocks, peptides are highly valuable due to their biodegradability, biocompatibility, low cytotoxicity, ease of manufacturing and tunability [15–17]. Peptide-based hydrogels are soft materials that show excellent injectability (thixotropic behaviour) [13], yielding suitable non-invasive materials for biomedical applications, including drug delivery, tissue engineering and regenerative medicine [15,18,19]. Amphipathic peptides, more particularly, characterized by the presence of alternating hydrophobic and hydrophilic side chains, usually self-assemble into β-sheets and subsequent β-sheet bilayers that are stabilized by non-covalent interactions, ultimately resulting in the formation of fibres and networks thereof [20,21].

We previously reported a set of short and tuneable amphipathic hexapeptide sequences that form self-supporting hydrogels in physiological saline solutions [22,23]. *In vivo* investigations have shown that gels composed of these peptide sequences, called hydrogelators hereafter, can serve as a suitable drug delivery platform for sustained release of therapeutically relevant molecules [24,25]. In the context of pain, various analgesics, including morphine and opioid peptides, have been successfully co-formulated with these hydrogelators (*e.g.* H-FQFQFK-NH_2) and their effectiveness was demonstrated in mice [22,25]. In addition, *in vivo* imaging studies allowed to visualize the stability ('residence time') of the hydrogel at the injection site as well as the release profile of various cargoes [24]. However, there is a need to further extend the drug release profile of these peptide-based delivery systems. We hypothesized that doubling the peptide length of the hexamer (H-FQFQFK-NH_2), to provide the dodecamer (H-FQFQFKFQFQFK-NH_2) (Fig. 1A), would increase the number of non-covalent interactions between the peptide chains (Fig. 1B) and slow-down *in vivo* hydrogel erosion. Moreover, it was anticipated that these increased intermolecular interactions would lead to different mechanical properties [14,26,27], which might also influence the cargo release after subcutaneous administration. Even though the influence of peptide length on hydrogel mechanical properties has been addressed in some specific cases [14,27–29], it is clear that a generalized conclusion on the influence of doubling the peptide length on mechanical properties of the hydrogel is lacking and, more importantly, the link to cargo release properties is not yet known.

Based on our hexamer (H-FQFQFK-NH_2, Fig. 1) core sequence, we first evaluated the effect of doubling the peptide length on fibre/network morphology and mechanical hydrogel properties (*i.e.* gel stiffness), which was performed using cryo- and negative staining transmission electron microscopy (TEM) and dynamic rheometry experiments. In order to evaluate the influence of doubling the hydrogelator length on the final drug release profiles, we performed *in vitro* release studies, *in vivo* imaging and *in vivo* efficacy experiments, as a validation step. This study is unique as we are the first to study the impact of doubling the peptide hydrogelator length on effective *in vivo* controlled drug release behaviour.

2. Materials and methods

2.1. Peptide synthesis and purification

Peptides were synthesized using the Fmoc-based solid-phase peptide synthesis (SPPS) strategy, either manually or using an automated microwave-equipped Peptide Synthesizer (Liberty Blue™ (CEM)). Rink amide AM resin (100–200 mesh, 0.92 mmol/g) was used as solid support, enabling the synthesis of *C*-terminal peptide amides. Amino acids (3 equiv) were coupled with O-(benzotriazole-1-yl)-*N,N,N′,N′*-tetramethyluronium hexafluorophosphate (HBTU, 3 equiv) and *N,N*-diisopropylethylamine (DIPEA, 6 equiv), in dimethylformamide (DMF) at room temperature (RT) for 45 min. As an exception, Boc-Dmt-OH (2 equiv) and Fmoc-6-aminohexanoic acid (2 equiv) were coupled with *N,N′*-diisopropyl carbodiimide (DIC, 2 equiv) and ethyl cyano(hydroxyimino) acetate (oxyma pure, 2 equiv), for 3 h and 2 h respectively, in DMF at

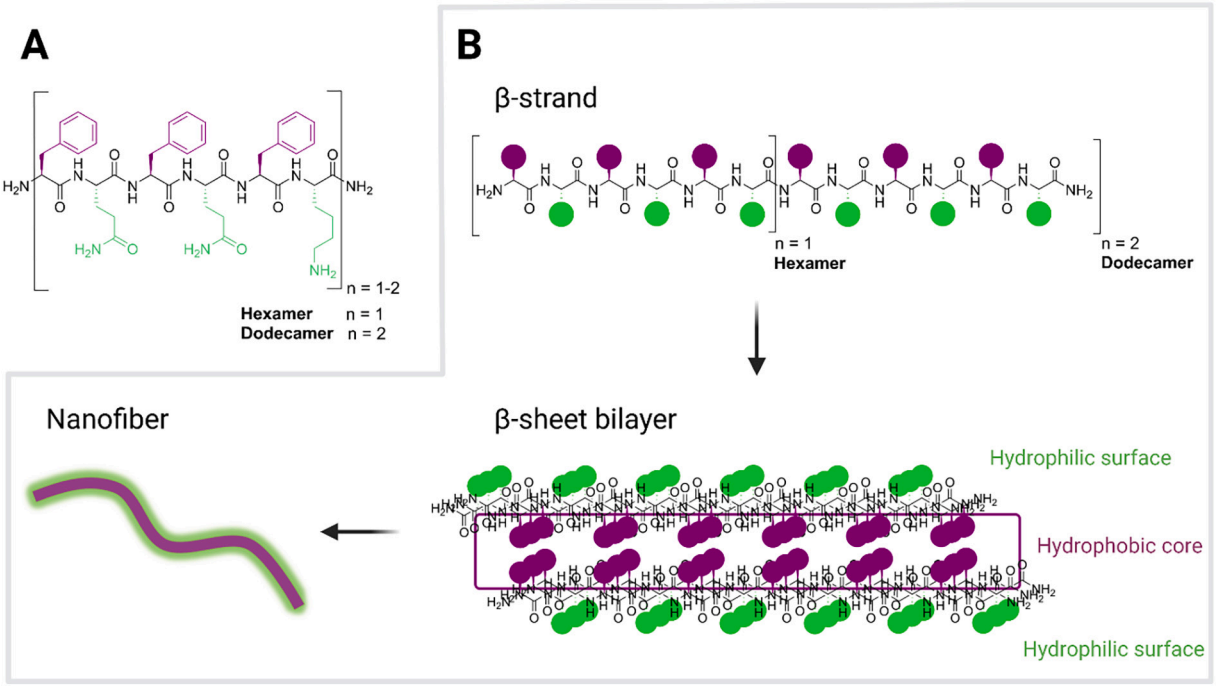

Fig. 1. (A) Chemical structure of the amphipathic peptide-based hydrogelators, with alternating hydrophobic amino acids (in purple) and hydrophilic amino acids (in green). (B) Illustration of the self-assembly process of amphipathic peptide-based hydrogelators. (For interpretation of the references to colour in this figure legend, the reader is referred to the web version of this article.)

RT. DOTA-labelled peptides were synthesized by activating DOTA-tris (tert-butyl ester) (1.5 equiv) with reagents DIC (1.5 equiv) and oxyma pure (1.5 equiv), in DMF, followed by an overnight coupling at RT. Deprotection of the Fmoc-group was conducted before amino acid coupling, using a solution of 4-methylpiperidine in DMF (20:80% v/v) (2×; 5 min and 15 min). All washing steps were performed with first DMF and then dichloromethane (DCM). To monitor the completion of each coupling reaction, Kaiser test was used, which is a qualitative colorimetric test displaying a yellow colour in case of a complete coupling [30]. After synthesis, the peptides were cleaved from the solid support together with side chain deprotections, by treatment with a mixture of trifluoroacetic acid (TFA), triisopropylsilane (TIS) and H_2O (95:2.5:2.5% v/v/v), for 3 h at RT. Afterwards, the cleavage solution was evaporated under reduced pressure and the crude mixture was dissolved using a solution of acetonitrile (ACN) and H_2O (50:50% v/v). After lyophilization, the crude peptide was dissolved in dimethyl sulfoxide (DMSO) and purified by preparative reversed phase high-performance liquid chromatography (RP-HPLC) (see Supporting Information). The collected pure fractions were combined and lyophilized to obtain the final compound with a purity of at least 97%. Lastly, the characterization and purity were confirmed using liquid chromatography-mass spectrometry (LC-MS) and high-resolution MS (HR-MS) (see Supporting Information). The synthesized hydrogelators and cargoes are summarized in Table 1.

2.2. ^{111}In-labelling of DOTA-labelled peptides

The labelling with Indium-111 (^{111}In) was performed as described previously [24]. Briefly, 1 mg DOTA-labelled peptide (cargo or hydrogelator) was dissolved in ammonium acetate buffer (NH_4OAc) (200 μL, 0.2 M, pH 5). Next, 25–38 μL of $^{111}InCl_3$ (20.0–23.5 MBq) was added and the mixture was incubated at 37 °C for 30 min. Lastly, the radiochemical purity (> 95%) was validated by instant thin layer chromatography (ITLC), using sodium citrate buffer (0.1 M, pH 5) as mobile phase.

2.3. Hydrogel preparation

2.3.1. For in vitro cargo release and cryo−/negative staining TEM

Stock solutions of the cargoes (TFA salt) were made first in phosphate-buffered saline solution (PBS) at the desired concentration (1 mg/mL or 2.2 mg/mL). Gelation was achieved by adding 100 μL of this stock solution to 2 mg of peptide hydrogelator (TFA salt) (2% w/v gel), in an Eppendorf tube (1.5 mL). All gels were then repetitively vortexed (1 min) and sonicated (5 min), after which they were left to rest overnight.

2.3.2. For dynamic rheometry

Cargoes (TFA salt) were first solubilized in PBS solution at the required concentration (1 mg/mL or 2.2 mg/mL). The hydrogel samples (2% w/v or 4% w/v), either unloaded or cargo-loaded, were prepared by adding PBS solution (pure or containing cargo) to the peptide hydrogelator powder (TFA salt), in a septum sealed glass vial. This was followed by repetitive vortexing (1 min) and sonication (5 min), after which the samples were aspirated in a 1 mL syringe and left to rest overnight. For analysis of the gel residue after *in vivo* injection, the hydrogel sample (2% w/v) was prepared as described in 2.3.1.

Table 1
Compound numbers and sequences of hydrogelators and cargoes used in this study.

Compound	Sequence
	HYDROGELATOR
1	H-Phe-Gln-Phe-Gln-Phe-Lys-NH_2
2	H-Phe-Gln-Phe-Gln-Phe-Lys-Phe-Gln-Phe-Gln-Phe-Lys-NH_2
3	DOTA-βAla-Phe-Gln-Phe-Gln-Phe-Lys-NH_2
4	DOTA-βAla-Phe-Gln-Phe-Gln-Phe-Lys-Phe-Gln-Phe-Gln-Phe-Lys-NH_2
5	SulfoCy5-Ahx-Phe-Gln-Phe-Gln-Phe-Lys-Phe-Gln-Phe-Gln-Phe-Lys-NH_2
	CARGO
C1	H-Ala-Ala-Gly-Ser-Ala-Trp-Tyr-Gly-Thr-Leu-Tyr-Glu-Tyr-Asp-β^{3}hTyr-NH_2
C2	DOTA-Ahx-Ala-Ala-Gly-Ser-Ala-Trp-Tyr-Gly-Thr-Leu-Tyr-Glu-Tyr-Asp-β^{3}hTyr-NH_2
C3	H-Dmt-DArg-Phe-Phe-NH_2
C4	DOTA-Ahx-Dmt-DArg-Phe-Phe-NH_2

2.3.3. For in vivo SPECT/CT imaging

2.3.3.1. In vivo hydrogel stability. Formation of the ^{111}In-labelled hydrogel was conducted by the addition of PBS to the ^{111}In-labelled hydrogelator solution described above (see 2.2.) until a volume of 1 mL was reached. To initiate the gelation process, 20 mg peptide hydrogelator (TFA salt) was added. The 2% w/v gel was formed almost immediately after repetitive vortexing (1 min) and sonication (5 min), after which it was left to rest overnight.

2.3.3.2. In vivo cargo release. PBS solution (pure or containing unlabelled cargo) was added to the ^{111}In-labelled cargo solution described above (see 2.2.) until a volume of 1 mL was obtained. Formation of the final hydrogel (loaded with ^{111}In-labelled cargo) was then achieved by adding the 1 mL cargo solution to 20 mg of peptide hydrogelator (TFA salt). The 2% w/v gel was formed almost immediately after repetitive vortexing (1 min) and sonication (5 min), after which the gel was left to rest overnight.

2.3.4. For in vivo efficacy - nociceptive assessment (hot-plate test)

A volume of 1 mL of 0.9% NaCl solution was added to the cargo (TFA salt), followed by addition of this solution to 20 mg peptide hydrogelator (TFA salt). The 2% w/v gel was formed almost immediately after repetitive vortexing (1 min) and sonication (5 min), after which the gel was left to rest overnight.

2.4. In vitro release studies

A volume of 500 μL of PBS solution (10 mM, pH 7.4) was heated at 37 °C for at least 30 min and then gently added on top of each cargo-loaded gel (= time-point 0). Samples of 10 μL or 20 μL were collected from the supernatant at regular time intervals after carefully homogenizing the solution and replaced by 10 μL or 20 μL fresh PBS solution (to maintain sink conditions). The collected samples were then analysed by analytical RP-HPLC (see Supporting Information). After determination of the area under the curve (AUC) values and making use of a calibration curve, the cumulative dose released (μg) (M_t) was calculated over time. Next, the cumulative release percentage (%) was determined using Eq. (1), with M_i being the initial encapsulated cargo dose. Finally, the acquired values were plotted over time in order to get the *in vitro* cargo release profile for each formulation. The experiment was performed in triplicate and data were presented as mean value ± standard deviation (SD).

$$\%Cumulative\ cargo\ release = \frac{M_t}{M_i}\ x\ 100 \quad (1)$$

2.5. Cryo- and negative staining TEM

2.5.1. Negative staining

Carbon-coated grids (EMSCF200H-CU-TH, ProSciTech) were glow discharged to render them hydrophilic. The hydrogels were prepared as described above (see 2.3.1.) and diluted with PBS (1:5) for a proper handling after overnight rest. 2 μL of this sample was then applied to an upturned grid held in anti-capillary forceps and left to adsorb for 1 min over moistened filter paper. Next, excess liquid was removed, and the grid was inverted onto a 30 μL drop of 2% phosphotungstic acid (PTA)

stain (pH 6.9) on Parafilm, for 1 min. Lastly, the grid was removed, after which the stain was wicked away with filter paper and allowed to dry before imaging. The hydrogel samples were examined using a Tecnai 12 Transmission Electron Microscope (FEI) at an operating voltage of 120 kV. Images were recorded using a FEI Eagle 4kx4k CCD camera and AnalySIS v3.2 camera control software (Olympus).

2.5.2. Cryo-TEM

A laboratory-built humidity-controlled vitrification grid plunge system was used to prepare the samples for Cryo-TEM. Humidity was kept close to 80% and ambient temperature was 22 °C. The hydrogels were prepared as described above (see 2.3.1.) and further diluted in PBS (1:10) after overnight rest for proper handling. An aliquot of 3 μL of this sample was then pipetted onto a 300-mesh copper grid coated with lacey formvar over a perforated carbon support (ProScitech, GSCu300FL-50C). After 10 s adsorption time, the grid was blotted manually using Whatman 541 filter paper, for approximately 2 s. The grid was then plunged into liquid ethane cooled by liquid nitrogen. Frozen grids were stored in liquid nitrogen until required. The samples were examined using a Gatan 626 cryoholder (Gatan) and Tecnai 12 Transmission Electron Microscope (FEI) at an operating voltage of 120 kV. At all times low dose procedures were followed, using an electron dose of 8–10 electrons/$Å^2$ for all imaging. Images were recorded using a FEI Eagle 4kx4k CCD camera and AnalySIS v3.2 camera control software (Olympus).

2.6. Dynamic rheometry

Dynamic rheometrical measurements were carried out with a Discovery HR-2 hybrid rheometer from TA Instruments equipped with a Peltier Plate and a Peltier Solvent trap containing Evaporation Blocker accessories. Temperature stability was assured by water cooling while mineral oil was used in the well to avoid solvent evaporation. All experiments were performed with a Solvent Trap 20 mm upper plate. Hydrogel samples were prepared as described in 2.3.2. and injected after overnight rest in between the rheometer plates, thereby keeping the gap size as low as possible to minimize water evaporation. The measurements were started with a 500 μm gap and followed a 5-step procedure for which a frequency of 0.15 Hz was applied as oscillation. The first step consisted of a 2 h time sweep at 25 °C, with a strain of 0.5%. Next, a temperature ramp from 25 °C to 37 °C was performed at 1 °C.min^{-1}, at a strain of 0.5%, to see the effect of temperature on the gel (step 2). Afterwards, a second time sweep at 37 °C and a strain of 0.5% was applied for 1 h (step 3). The gel was then destroyed by a strain ramp from 0.01% to 500% (step 4), followed by the study of the subsequent recovery of the gel. For this, a last time sweep at 37 °C and a strain of 0.5% for 2 h was finally performed (step 5). For analysis of the gel residue after *in vivo* injection, 150 μL of the hydrogel sample (prepared as described in 2.3.1.) was injected subcutaneously just above the right hind limb of a female C57BL/6 J mouse. The mouse was killed at 6 h post-injection, after which the remaining gel residue was taken out and analysed immediately using dynamic rheometry. For this, the dissected gel was transferred to the Peltier plate using a spatula. The upper plate was lowered to a gap of 150 μm and the measurement started following the same 5-step procedure as just described.

2.7. In vivo SPECT/CT imaging

Protocols were approved by the Ethics Committee for Animal Experiments of the Vrije Universiteit Brussel (project numbers: 19–272-25, 20–272-13, 20–272-22) and subjected to the provisions of the Royal Decree of 29 May 2013 concerning the protection of animals used for scientific purposes and the Regulations of the Ethics Committee for Animal Experiments. Female C57BL/6 J mice (from Charles River, L'Abresle, France) were used, with 3 or 4 mice per group (for stability and cargo release experiment respectively). The mice were housed in individually ventilated cages at 19–24 °C in 40–60% humidity with a light/dark cycle of 14/10 h. Food pellets and water were provided *ad libitum*. Before the start of the experiment, the mice were acclimatized to the new environment for at least one week. All experimental procedures were performed under 2–5% isoflurane anaesthesia, with an oxygen flow rate of 0.5–1.5 L/min. Body condition score, animal behaviour and physical appearance were daily checked. At the end of the study, mice were killed by cervical dislocation.

A volume of 150 μL of the 2% w/v hydrogel (^{111}In-labelled hydrogel or hydrogel loaded with ^{111}In-labelled cargo) (see preparation in 2.3.3.) (1.55–3.63 MBq) was injected subcutaneously just above the right hind limb of the mice. Animals were then subjected to non-invasive SPECT/CT scans at different time-points post-injection (0, 3, 6, 12, 24, 48 and 72 h for the *in vivo* release experiments and 0, 1, 2, 3, 4, 6 and 8 days for the *in vivo* stability experiment). SPECT/CT imaging was performed on a Vector+ system (MiLabs) equipped with a general-purpose rat/mouse 1.5 mm 75 pinhole collimator. Scans were performed in spiral mode with 6 bed positions and an acquisition time of 200 s per bed position. For image reconstruction, 2 subsets and 4 iterations were used, with a voxel size of 0.4 mm, in U-SPECT-Rec software (Milabs). The CT scan was made in 1 bed position, with a duration of 146 s at 60 kV and a pixel size of 80 μm. The acquired images were processed and quantified using the AMIDE software. More specifically, all images were equally scaled (0–100% ID/cc and 0–250% ID/cc for the *in vivo* release and stability experiment respectively) and a region of interest (ROI) was drawn around the injection site of the hydrogel. The total radioactivity within this ROI was then calculated and expressed as percentage of injected dose (% ID/cc) remaining as a function of time. All data were presented as mean value ± SD. Statistical analysis was done to compare the two groups (hydrogel **1** and **2**) at different time-points, using a mixed effects two-way ANOVA with a correction for multiple comparisons *via* the Holm-Sidak method (GraphPad Prism 8.0 software). *P*-value <0.05 was considered significant. 3D maximum intensity projections (MIP) images were prepared in Osirix (Pixmeo).

2.8. In vivo efficacy - nociceptive assessment (hot-plate test)

Experimental protocols were carried out within the ethical guidelines established by the National Institute of Health and approved by Paris-Descartes University ethics committee for animal experimentation (No. APAFIS#24469-20190705102639v2). Male Swiss mice (Janvierlabs, France) weighing 35–40 g at the time of experimentation were used. The mice were housed in well-ventilated cages at 19–24 °C in 40–60% relative humidity with 12 h light/dark cycle and free access to food and water for at least one week before the experiments. The hot-plate test was used as described by Eddy and Leimbach (1953) [31], to assess antinociceptive effects of the different formulations in mice after subcutaneous administration in the flank. A glass cylinder was used to restrain the mouse on the heated surface of the plate, which was kept at a temperature of 52 °C (Bioseb, France). The latency period until the mouse jumped or shacked/withdrawn/licked its paws was registered, using a cut-off time of 30 s. Latencies were measured 3 times before (basal latency) and at 5, 15, 30 min, 1, 2, 3, 4, 5, 6, 7, 8, 9, 24, 48, 72 and 96 h (test latency) after subcutaneous injection of the hydrogel co-formulations (5 μL/g) or immediate release formulations (5 μL/g). Each experimental group included 5 mice. The percentage of analgesia was calculated based on the following equation (Eq. (2)):

$$\%Analgesia = \left[\frac{test\ latency - basal\ latency}{cutoff\ time - basal\ latency}\right] \times 100 \quad (2)$$

All experimental data were expressed as mean value ± SD. Data were statistically evaluated using a two-way ANOVA Bonferroni *post hoc* test (GraphPad Prism 8.0 software). Individual AUC values for analgesia were calculated by the trapezoid method from time-point 0 to 96 h. Statistics on these data was performed using a one-way ANOVA

Bonferroni *post hoc* test (GraphPad Prism 8.0 Software). *P*-value <0.05 was considered significant.

3. Results and discussion

3.1. Peptide design

Amphipathic peptides, bearing alternating hydrophobic and hydrophilic amino acids (as illustrated in Fig. 1A), have a high tendency to form β-sheets upon adding physiological solutions, as demonstrated by FT-IR spectroscopy (Fig. S1). These will further self-assemble into nanofiber networks (Fig. 1B) [20,26,32]. Our recent findings have shown that amphipathic hexapeptide hydrogelator **1** (H-FQFQFK-NH_2, Table 1) displayed promising properties as controlled drug delivery vehicle. More specifically, its efficacy was demonstrated by an effective and prolonged painkilling effect after subcutaneous administration of the hydrogel co-formulated with the analgesic cargo **C3** (H-Dmt-DArg-Phe-Phe-NH_2) [25]. Aiming at an extension of the current release timeframe of the encapsulated drug, we envisioned to increase the hydrogelator length. Therefore, starting from hexapeptide **1** as lead sequence (Fig. 1A, n = 1), we prepared the corresponding dodecapeptide, hydrogelator **2** (H-FQFQFKFQFQFK-NH_2) (Fig. 1A, n = 2). This design allowed to study the influence of increased intermolecular interactions on the self-assembly kinetics and mechanical properties of the hydrogels, and eventually on the cargo release after subcutaneous administration.

3.2. In vitro release studies

The drug release properties of hydrogels composed of peptides **1** and **2** have been evaluated by static *in vitro* release experiments, involving different cargoes. Even though the *in vitro* setting is not fully representative of the complex *in vivo* environment, it allows to obtain information on the ability of the hydrogels to retain the drugs and provoke sustained drug release. At the start of the experiment, a PBS solution of 37 °C (pH 7.4) was gently added on top of the cargo-loaded hydrogel, serving as a physiologically relevant release medium. Throughout the whole experiment, a temperature of 37 °C has been maintained, simulating the *in vivo* setting. The first cargo investigated is the pentadecapeptide **C1** (Table 1), originally designed as a nanobody CDR peptidomimetic [33,34], serving as middle size peptide cargo in the present study. Surprisingly, only a slight initial release was observed within the first 6 h, for both hydrogels **1** (in blue) and **2** (in red), as shown in Fig. 2A (rhombus symbols). Since no further release was detected within 48 h, a large portion of the cargo is likely to be retained within both gel networks. Interestingly, this observation indicated that **C1** would only be released upon *in vivo* degradation/erosion of the gels. Next, the release of the bioactive opioid peptide **C3** [25] was examined. In Fig. 2A (triangle symbols), the release profile from hydrogel **1** and **2** is presented, indicating a more rapid burst release within the first 30 min (*ca.* 27% and 20% respectively), followed by a more gradual and sustained release profile. From 24 h until 48 h, a slow release was still noted, up to complete release from both hydrogel networks. Overall, the *in vitro* release profile of **C3** was quite similar for both hydrogel **1** and **2**. However, when comparing the release curves of **C1** and **C3** it was noteworthy that the smaller opioid peptide **C3** is released faster from both hydrogel networks.

Because *in vivo* nuclear imaging experiments were planned afterwards, the *in vitro* release of **C1** and **C3** modified with an imaging label (*i.e.* chelator) was studied as well, allowing to assess the impact of the chelator on the release behaviour. To this end, cargoes **C2** and **C4** were synthesized as modified analogues of **C1** and **C3** (Table 1), bearing a chelator (DOTA) linked to the *N*-terminus through an aminohexanoic acid moiety (Ahx). The *in vitro* release of **C2** from hydrogels **1** and **2** is presented in Fig. 2B (circle symbols), indicating similar release profiles as for the unmodified peptide **C1**. Regarding the release of the modified

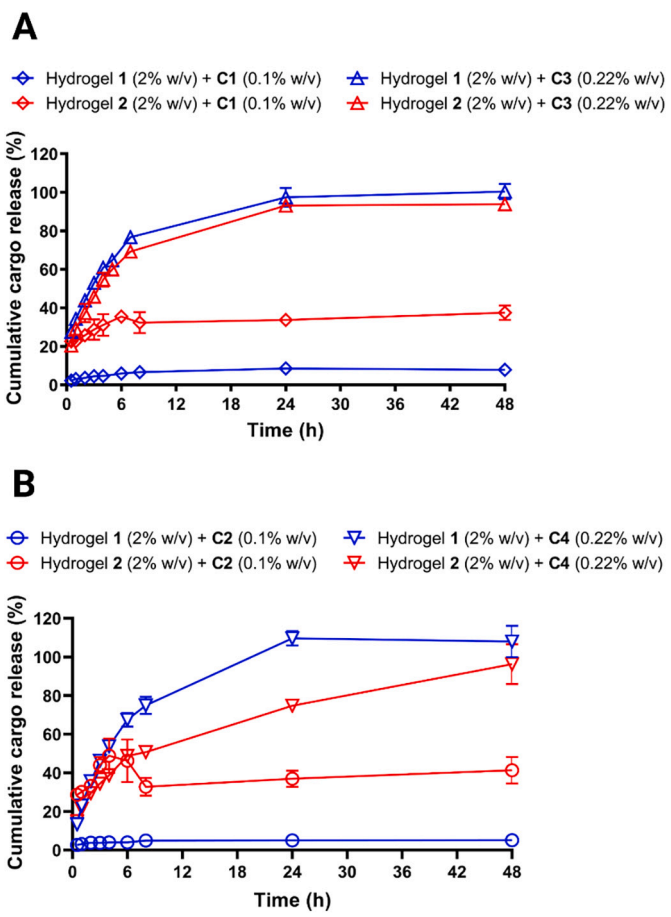

Fig. 2. *In vitro* release of peptide cargoes from peptide-hydrogels **1** (in blue) and **2** (in red) (2% w/v in PBS). (A) Release of cargo **C1** and **C3**, co-formulated with the hydrogelators in a 1 mg/mL and 2.2 mg/mL concentration respectively. Data points representing mean values ± SD (n = 3). (B) Release of cargo **C2** and **C4**, co-formulated with the hydrogelators in a 1 mg/mL and 2.2 mg/mL concentration respectively. Data points representing mean values ± SD (n = 3). Lines are drawn to guide the eye. (For interpretation of the references to colour in this figure legend, the reader is referred to the web version of this article.)

opioid peptide **C4** from hydrogel **1** and **2**, the results are depicted in Fig. 2B (triangle symbols) and show a limited burst release of 13% and 15% respectively, and a further sustained release for both hydrogels. Complete release is obtained after 24 h and 48 h for hydrogel **1** and **2** respectively, indicating a slower sustained release for hydrogel **2**. Altogether, the *in vitro* release profiles of the chelated peptides **C2** and **C4**, after comparison to their corresponding native sequences (**C1** and **C3** respectively), demonstrated the limited impact of the imaging labels on the cargo release behaviour from peptide hydrogels **1** and **2**.

3.3. Hydrogel characterization

3.3.1. Cryo- and negative staining TEM

Cryo-TEM and negative staining TEM experiments were performed to visualize and characterize the hydrogel networks, revealing information on the fibre morphology and associated self-assembly mechanism. In Fig. 3, the negative stain and cryo-TEM images of peptide hydrogels **1** and **2** are shown, indicating that both hydrogelators are able to form an extensive nanofiber network, with clear differences observed in fibre morphology. Hydrogel **1** showed an abundance of very long flexible fibres intertwined into a fibrous network. A linear aggregation into tape like structures is suggested, since both fine fibrils as well as a broader appearance along the fibre length was observed. The fibres are approximately 2 nm in width, which is similar to what was previously

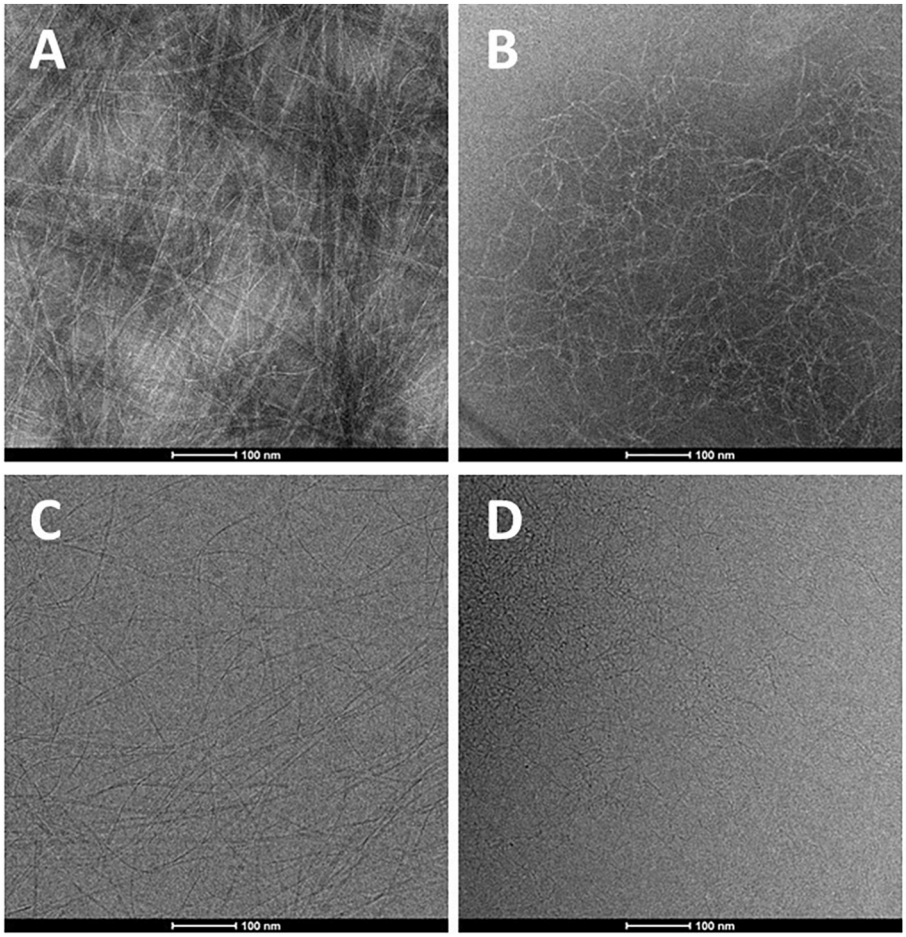

Fig. 3. Negative stain TEM images of (A) hydrogel **1** and (B) hydrogel **2** and cryo-TEM images of (C) hydrogel **1** and (D) hydrogel **2** (2% w/v gels in PBS), showing the hydrogel's fibre morphology and self-assembled nanofibrous network. Scale bars represent 100 nm.

observed for gels composed of hydrogelator peptide H-FEFQFK-NH_2 [22]. Hydrogel **2** has a markedly different appearance with significantly shorter fibrils than hydrogel **1.** The tangled network indicates flexibility of the fibres and small circular features were also observed, suggesting a degree of terminal aggregation. The fibres were approximately 2 nm in width and appeared more disordered (less "ribbonlike") than those observed for hydrogel **1**. These results suggest that increasing the length of the primary peptide sequence imparts an effect on linear alignment and fibre length during the self-assembly process. Both hydrogels are composed of highly intertwined fibrous networks underpinning the stability of the self-assembled structures. Additional cryo-TEM and negative stain TEM images can be found in the Supporting Information (Figs. S2 & S3).

3.3.2. Dynamic rheometry: mechanical properties and thixotropy

The mechanical properties of the hydrogels in this study were assessed using dynamic rheometry, with a 5-step procedure as described in Section 2.6. Fig. 4A shows a typical rheological measurement for the hexapeptide hydrogel **1** and the dodecapeptide hydrogel **2**, both unloaded and loaded with cargo **C2**. Specifically, the hydrogel samples were injected in between the rheometer plates after an overnight rest in a syringe. In a first step, the recovery of the gel after injection was followed at 25 °C for 2 h. In step 2 and 3, the temperature effect was studied by a temperature scan from 25 °C to 37 °C, followed by an isothermal time sweep at 37 °C for 1 h. Finally, the hydrogel was destroyed *in situ* by shearing at 37 °C (step 4), followed by a second recovery during 2 h at 37 °C (step 5). The results are represented in Fig. 4. Additionally, the reproducibility of all experiments (in triplicate), together with the loss moduli (G") profiles and the results of the co-formulation with cargo **C4**/**C3** are included in the Supporting Information (Figs. S4-S12). The reproducibility of the results and the plateau values of the moduli reached in both recovery steps (steps 1 and 5, Fig. 4A-B) confirm the efficiency of the solvent trap used in the experimental set-up. Some general conclusions regarding mechanical properties (gel stiffness), temperature effect and recovery behaviour (thixotropy) can be drawn from the experiments. As summarized in Fig. 4C, the storage moduli of the 2% w/v dodecapeptide hydrogels **2** and **2** + **C2** are well below 100 Pa and substantially lower than the corresponding hexapeptide systems **1** and **1** + **C2**, *i.e.* a factor of >10 (unloaded) and >60 (loaded), respectively. For the same peptide concentration (% w/v), the network structure of hydrogel **2** might be looser with a bigger cavity (mesh) size, less entanglements and a lower cross-linking density, due to the lower number of associating peptide hydrogelators in solution, which seems in agreement with the TEM images (Fig. 3). While the smaller cargo **C4**/**C3** has a similar effect on the mechanical properties of hydrogels **1** and **2** (more or less doubling the storage modulus), the bigger cargo **C2** has a completely different effect. Indeed, while the modulus of hydrogel **1** is increased by a factor 5 (up to *ca.* 3300 Pa), the modulus of hydrogel **2** stays almost constant around 55 Pa.

The temperature effect (step 2 and 3 in Fig. 4A) is limited in all systems. A slight decrease in modulus is noticed in the temperature scan from 25 °C to 37 °C, which is then compensated by a slight increase with time if the temperature is kept constant at 37 °C. This systematic trend was not further investigated. Overall, in this study the mechanical properties of the dodecapeptide hydrogel **2** are clearly lower than these of the hexapeptide hydrogel **1** (Fig. 4C). However, next to the

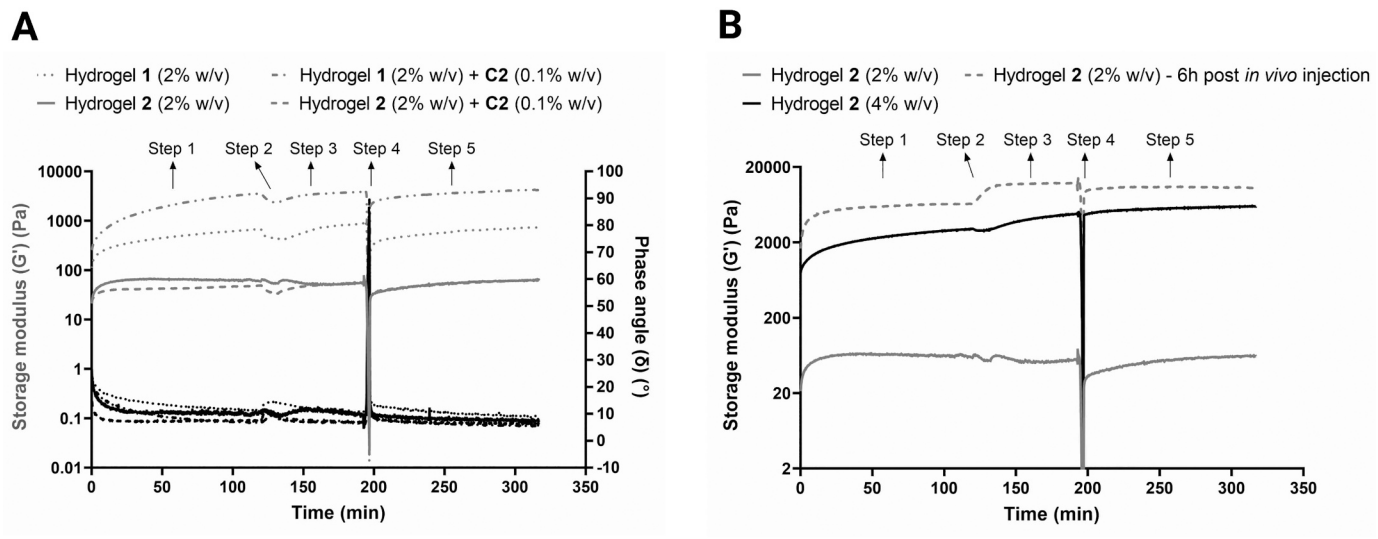

C

HYDROGEL 1	G' (Pa) ± SD
H1 (2% w/v)	660 ± 160
H1 (2% w/v) + C2	3330 ± 1040
H1 (2% w/v) + C4/C3	1050 ± 350
H1 (4% w/v)	6170 ± 1080

HYDROGEL 2	G' (Pa) ± SD
H2 (2% w/v)	60 ± 10
H2 (2% w/v) + C2	50 ± 10
H2 (2% w/v) + C4/C3	150 ± 90
H2 (2% w/v), 6 h post-injection	6470
H2 (4% w/v)	3480 ± 400

Fig. 4. Mechanical characterization of unloaded and cargo-loaded peptide-hydrogels, using dynamic rheometry with a 5-step procedure: time sweep at 25 °C after injection (first recovery), temperature scan up to 37 °C, time sweep at 37 °C, strain sweep (*in situ* destruction at 500% strain) and time sweep at 37 °C (second recovery). (A) Rheological measurement (storage modulus (in grey) and phase angle (in black)) of hydrogel **1** and hydrogel **2** (2% w/v in PBS), both without and with cargo **C2** (0.1% w/v). (B) Rheological measurement (storage modulus) of hydrogel **2** at 2% w/v and 4% w/v gel concentration, and hydrogel **2** (2% w/v) at 6 h post *in vivo* injection. (C) Overview of the storage moduli (G') ± SD of the respective measurements. All values were reported at the end of step 1 (time sweep 2 h).

comparison of shorter and longer chain lengths, also the concentration of the hydrogelators (expressed in % w/v) is important. This concentration effect was examined for both hydrogels by measuring the G' value of both a 2% w/v and 4% w/v gel (Fig. 4B-C). The increase of the modulus at 25 °C along with peptide concentration is more pronounced for hydrogel **2** (from *ca.* 60 to 3480 Pa) than for hydrogel **1** (from *ca.* 660 to 6170 Pa). The steeper increase of the G' of hydrogel **2** with peptide concentration can be explained by the shorter length of the dodecapeptide fibrils (see TEM results), resulting in the need of a higher concentration to increase the cross-linking density. Therefore, a generic correlation describing the effect of the length of the primary peptide sequence on the hydrogel's storage modulus is not straightforward and will for instance depend on the specific nature of the peptide sequence and the peptide hydrogelator concentration. The phase angle (δ) measured during the full 5-step procedure is also represented in Fig. 4A. More specifically, the phase angle stays mostly below 10°, indicative for a dominant elastic behaviour of the hydrogels, even for the lowest modulus values. In contrast, during shear destruction (strain sweep in step 4 up to 500% strain) G' almost drops to zero and δ tends to 90°, proving the network destruction which led to an almost purely viscous deformation, that is crucial for a proper injectability of the peptide hydrogel. Initial recovery of the viscous liquid to a stable hydrogel is very fast for both hydrogels. The full recovery of the hydrogels to reach a plateau value in G' after destruction, as visualized in steps 1 and 5, leads to elastic responses and stabilized moduli are regained, revealing two important observations: 1) the full recovery of the gel after shear and elongational flow by injection through the needle of the syringe (step 1) takes more time than the recovery after pure shear destruction *in situ* in between the plates of the rheometer (step 5 in Fig. 4); 2) the full recovery is faster in the dodecapeptide systems than in the hexapeptide systems (Fig. S6). This means that thixotropy is less pronounced in hydrogel **2**, leading to a shorter recovery time after destruction, which might be important for the cargo release properties. Indeed, after injection the re-encapsulation of the cargo inside the hydrogel might be faster allowing a slower release (*vide infra*).

3.3.3. *Dynamic rheometry: post in vivo injection mechanical properties*

The less pronounced thixotropy observed in hydrogel **2** might favour a slower cargo release, as mentioned above. However, linking the lower mechanical stiffness of this dodecapeptide hydrogel, as measured in PBS solution *before* injection, to a different *in vivo* cargo release profile *after* injection of the same hydrogel concentration (2% w/v) remains challenging. To address this challenging question, the rheological (mechanical) properties of an unloaded hydrogel based on the self-assembly of **2** *after in vivo* injection were measured. The mouse was dissected 6 h after injection and the recovered hydrogel was measured in almost identical rheological conditions as the freshly prepared ones. Only the gap between the plates was lowered to accommodate the reduced amount of hydrogel (subcutaneous injections of 150 μL are applied in mice). The '6 h post-injection' storage modulus of hydrogel **2** is shown in Fig. 4B together with G' curves at different concentrations pre-injection. The post-injection modulus (*ca.* 6500 Pa) is remarkably increased and at least 100 times higher than the pre-injection modulus (*ca.* 60 Pa), exceeding the G' values of hydrogel **2** at 4% w/v (*ca.* 3500 Pa) and hydrogel **1** in combination with **C2** (*ca.* 3300 Pa), and is similar to that of hydrogel **1** at 4% w/v (*ca.* 6200 Pa, Fig. 4C). This post-injection effect was measured for the first time in this work and more research is needed for a thorough understanding of its impact on release properties.

Nevertheless, it is clear that determination of the hydrogels' mechanical properties only before injection is not sufficient to rationalize the *in vivo* cargo release profiles measured in this study. Therefore, post *in vivo* injection measurements seem a very interesting approach to gain additional insights.

3.4. In vivo SPECT/CT imaging

After the *in vitro* validation of the systems, the hydrogels have been further investigated by means of *in vivo* imaging studies. First, the stability of the two hydrogel systems was evaluated using non-invasive SPECT/CT imaging. Specifically, injection of the hydrogel composed of hexapeptide hydrogelator **1** was compared to the one formed by dodecapeptide hydrogelator **2**. DOTA was covalently coupled to both sequences, using a β-alanine amino acid as linker, resulting in hydrogelators **3** and **4**, respectively (Table 1). The presence of the DOTA chelator enabled radiolabelling with the radioactive isotope ^{111}In, hence allowing the visualization of the injected hydrogels *via* SPECT monitoring. Practically, the hydrogel network was formed applying a mixture of 1:20 **3**/**1** and **4**/**2** (for hexapeptide- and dodecapeptide-based gels, respectively). After subcutaneous injection of the ^{111}In-labelled hydrogel (150 μL), the radioactive signal at the injection site was followed over time, providing an estimation of the remaining hydrogel volume. For hydrogel **2**, 87% of the initial hydrogel volume was still present at the injection site after 8 days, which is in stark contrast to hydrogel **1**, where the largest decrease in volume was observed already after 24 h (Fig. 5A). Only 23% of the hydrogel volume (hydrogelator **1**) was still present 2 days post-injection, which is comparable to previous results obtained with hexapeptide H-FEFQFK-NH_2 [24]. In summary, this experiment clearly demonstrated the improved *in vivo* stability of the dodecapeptide hydrogel **2** compared to its hexapeptide counterpart **1**, while being still biodegradable as evidenced by *in vivo* fluorescence imaging studies (Fig. S13).

In vivo release experiments using non-invasive SPECT/CT imaging were carried out to evaluate whether the observed increased stability of hydrogel **2** also leads to a more prolonged *in vivo* drug release time. To this end, two peptide cargoes (**C2** and **C4**, Fig. 6) were co-formulated separately within hydrogel **1** and **2**.

First, the *in vivo* release of peptide **C2** was studied. The ^{111}In-labelled cargo was incorporated in both hydrogels at a concentration of 1 mg/mL

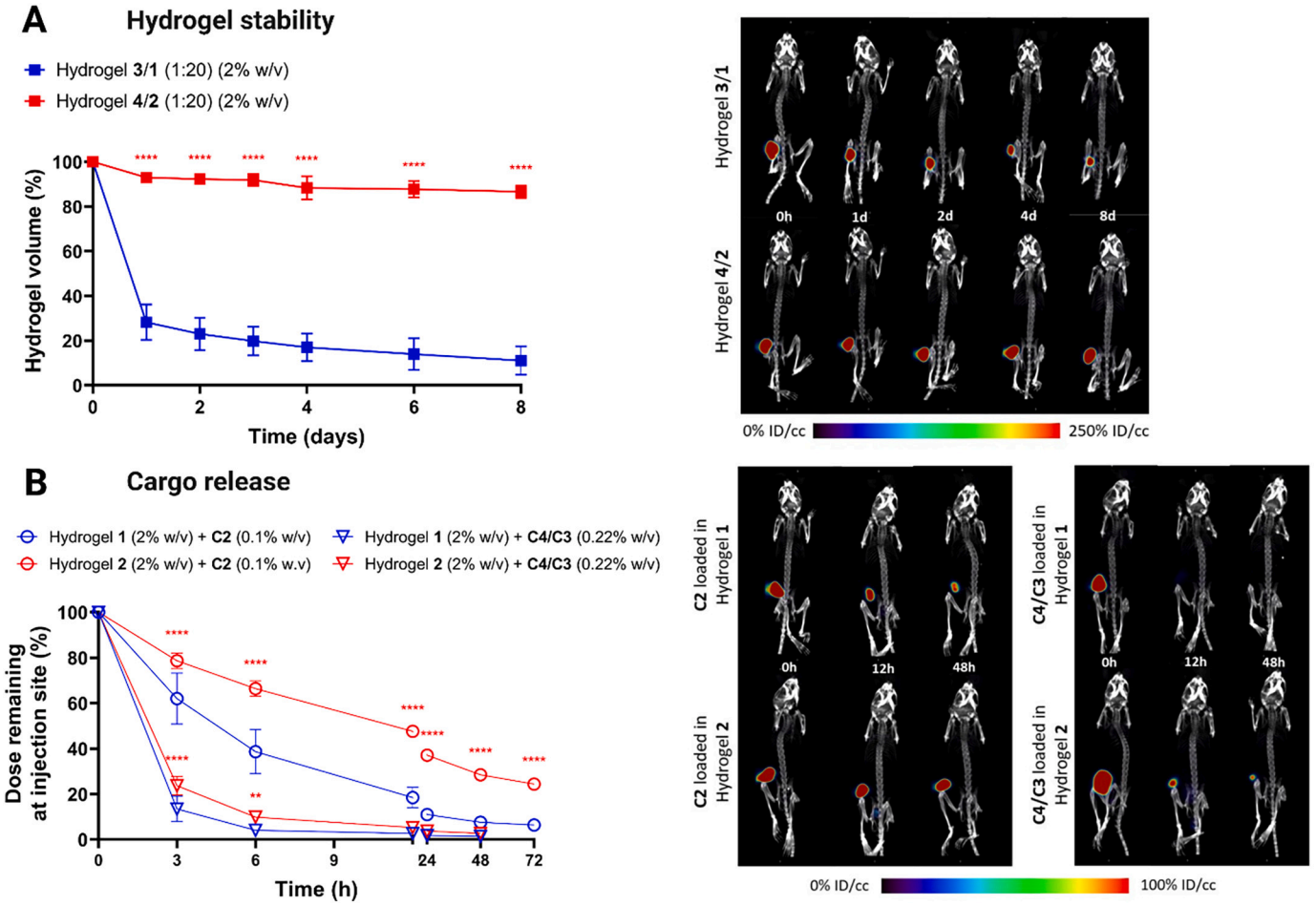

Fig. 5. *In vivo* imaging of unloaded and cargo-loaded peptide-hydrogels, *via* nuclear SPECT/CT imaging after subcutaneous injection in mice. (A) *In vivo* stability profile (left) of hydrogels **3**/**1** (1:20) (in blue) and **4**/**2** (1:20) (in red) (2% w/v in PBS, of which 0.1% w/v is radioactively labelled). The remaining radioactive signal at the injection site was quantified at different time-points post-injection, representing hydrogel stability over time. Data points presenting mean values ± SD (n = 3): (****) $P < 0.0001$ hydrogel **4**/**2** *vs.* hydrogel **3**/**1**. SPECT/CT images (right) taken at different time-points after subcutaneous injection of the hydrogels. All images were scaled to the same level (0–250 %ID/cc). (B) *In vivo* release profile (left) of **C2** and **C4**/**C3** (1:1.2) from hydrogels **1** and **2** (2% w/v in PBS). Cargo **C2** and cargo mixture **C4**/**C3** (1:1.2) were co-formulated with both hydrogelators in a 1 mg/mL and 2.2 mg/mL concentration respectively. The radioactive signal at the injection site was quantified at different time-points post-injection, representing the remaining dose over time, presented as mean ± SD (n = 4): (**) $P < 0.01$, (****) $P < 0.0001$, hydrogel **2** *vs.* hydrogel **1**. SPECT/CT images (right) taken at different time-points after subcutaneous injection of the respective co-formulations. All images were scaled to the same level (0–100 %ID/cc). (For interpretation of the references to colour in this figure legend, the reader is referred to the web version of this article.)

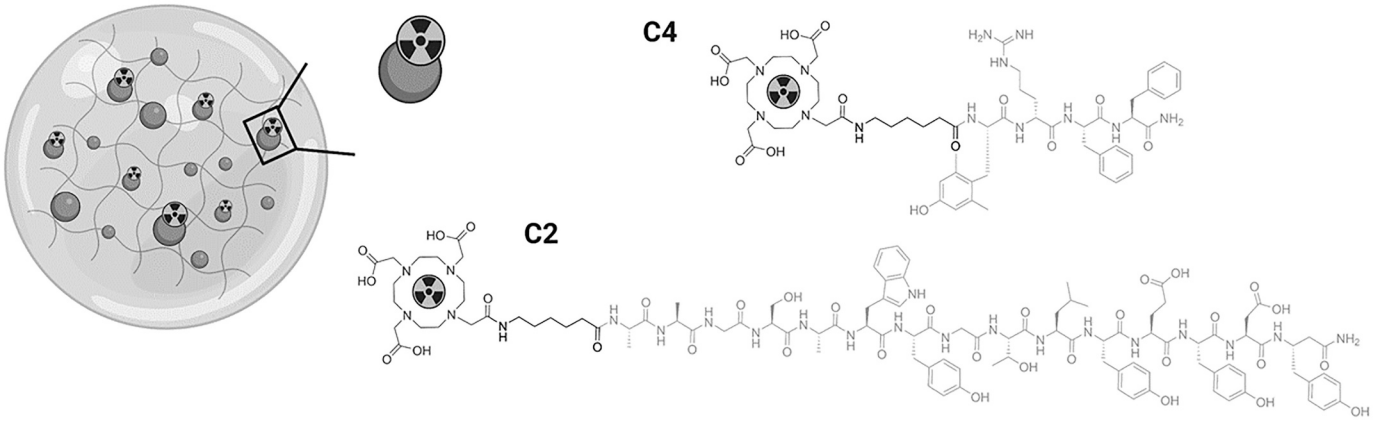

Fig. 6. Illustration of the encapsulation of radioactively labelled cargoes **C4** and **C2** within a hydrogel network. Structures of the two cargoes are shown, indicating the DOTA chelator, which is chelating the radioactive isotope ^{111}In, represented by the radioactive symbol. The peptide structure is indicated in grey and the Ahx linker in black. (For interpretation of the references to colour in this figure legend, the reader is referred to the web version of this article.)

(0.1% w/v). A volume of 150 μL of this cargo-loaded gel was then injected subcutaneously, just above the right hindlimb of the mice, after which the remaining radioactivity could be determined at the injection site over time, hence providing the duration of *in vivo* drug release from both hydrogels. As expected, the cargo was released from hydrogel **2** in a sustained way until at least 72 h, which is significantly more extended as compared to the release from hydrogel **1**, for which almost all cargo was released at 24 h post-injection (Fig. 5B). In view of these promising results and considering future clinical applications in the field of pain-killing, the *in vivo* release of the potent analgesic **C3** was investigated as well, using the modified version **C4** (described above) considering the required radiolabelling (Table 1). Specifically, 1 mg of **C4** was successfully labelled with radioisotope ^{111}In, after which 1.2 mg of **C3** was added to reach a total clinically relevant dose of 18.7 μmol/kg (0.22% w/v). The ^{111}In-labelled **C4**/**C3** mixture (1:1.2) was co-formulated in the two hydrogel systems and the release was followed until 48 h post-injection. As illustrated in Fig. 5B, hydrogel **2** provides a significantly slower release compared to hydrogel **1**, demonstrating the potential of hydrogel **2** to further slow-down the analgesic drug release (this was subsequently demonstrated *via in vivo* antinociceptive measurements, *vide infra*). Of note, the overall release of **C4**/**C3** from both gels is clearly faster compared to **C2**, highlighting the importance of the physicochemical properties of the two cargoes on the release kinetics, as already demonstrated through the *in vitro* release studies. Altogether, these findings indicate that the hydrogel system (sequence, length, concentration, etc.) as well as the properties of the encapsulated cargo have a crucial impact on the stability of the gels and the corresponding release kinetics. Nonetheless, for both cargoes the promise of doubling the hydrogelator length with the aim to prolong the drug release time was successfully confirmed.

Previous studies unveiled that the main drug release mechanism of the hexapeptide hydrogelator H-FEFQFK-NH_2 appeared to be based on a degradation/erosion mechanism, rather than being linked to the proteolytic (in)stability of the peptide gelators [24]. This conclusion was drawn from past experiments involving stabilized D-amino acid- and β-amino acid-containing peptide gelators, for which we did not see significant differences in release kinetics, while their proteolytic stability was higher than standard α-amino acid-bearing sequences [22]. In the current study, the erosion model is confirmed for hydrogel **1** (H-FQFQFK-NH_2), as both cargoes **C4** and **C2** are released within approximately the same time of hydrogel disappearance from the injection site (*ca.* 24 h). Hydrogels composed of the dodecamer **2**, however, are more stable *in vivo* (Fig. 5A). This observation can be rationalized by the increased number of supramolecular (non-covalent) interactions between dodecamer **2** peptides within the nanofibers, as compared to hexamer **1** peptides, eventually leading to stronger peptide fibres in case of dodecamer **2**. This hypothesis is further supported by a decreased release of hydrogelator **2** *versus* hydrogelator **1**, as observed in *in vitro* release experiments (Fig. S16). These experiments allowed, next to the release of the studied cargoes, to quantify the amount of hydrogelator released in the supernatant, as an indication of fibre stability. Note that the higher stability, and slower erosion, of the hydrogel composed of dodecamer **2** indicates stronger supramolecular interactions within the peptide nanofibers. Importantly, however, and as suggested by Fig. 5B, the physicochemical properties of the cargo also play a role in the release kinetics, most probably through non-covalent cargo-peptide fibre interactions, as very recently suggested by Elsawy and coworkers [35].

3.5. *In vivo efficacy - nociceptive assessment (hot-plate test)*

To evaluate the extended-release efficacy of the hydrogelator systems as a controlled drug delivery platform, an acute thermal nociception model (*i.e.* hot-plate test) was applied after subcutaneous administration of formulations containing opioid peptide **C3** or morphine in mice. While the effectiveness of hydrogel **1** (H-FQFQFK-NH_2) was proven in a previous study [25], our objective was to prolong the antinociceptive effects, aiming at a more consistent pain control and overall quality of life for patients suffering from chronic pain. In this study, groups of mice (n = 5) received **C3** (74 μmol/kg) co-formulated with hydrogel **1** or **2** (2% w/v), **C3** (74 μmol/kg) applied in 0.9% NaCl, morphine (100 μmol/kg) in 0.9% NaCl or 0.9% NaCl (negative control). The results are represented in Fig. 7 and it can be clearly noted that the co-formulations facilitate prolonged antinociceptive effects compared to the immediate release formulations of the opioid cargoes (**C3** or morphine in 0.9% NaCl, green and purple curves/bars in Fig. 7A/B respectively). Additionally, the higher AUC for hydrogel **2** compared to hydrogel **1** (Fig. 7B) indicates a more sustained release of cargo **C3** when encapsulated in the double length hydrogelator, again strengthening the proposed hypothesis that increased hydrogelator lengths can provide a higher hydrogel stability, which consequently leads to prolonged clinical effects.

Finally, the biocompatibility of the two hydrogelators has been further validated through additional *in vitro* and *in vivo* data. The *in vitro* immunogenicity has been investigated using a pro-inflammatory Meso Scale Discovery (MSD) cytokine assay. The concentration of cytokines gives an idea of the local inflammatory response to the hydrogels. While LPS, as a pro-inflammatory agent, increases the concentration of several inflammation markers, such as IFN-γ, TNF-α and different interleukins, the two hydrogelators do not present this behaviour (at 100 μM) (Fig. S14A). Interestingly, cell viability was also maintained upon treating peripheral blood mononuclear cell (PBMCs) with the two

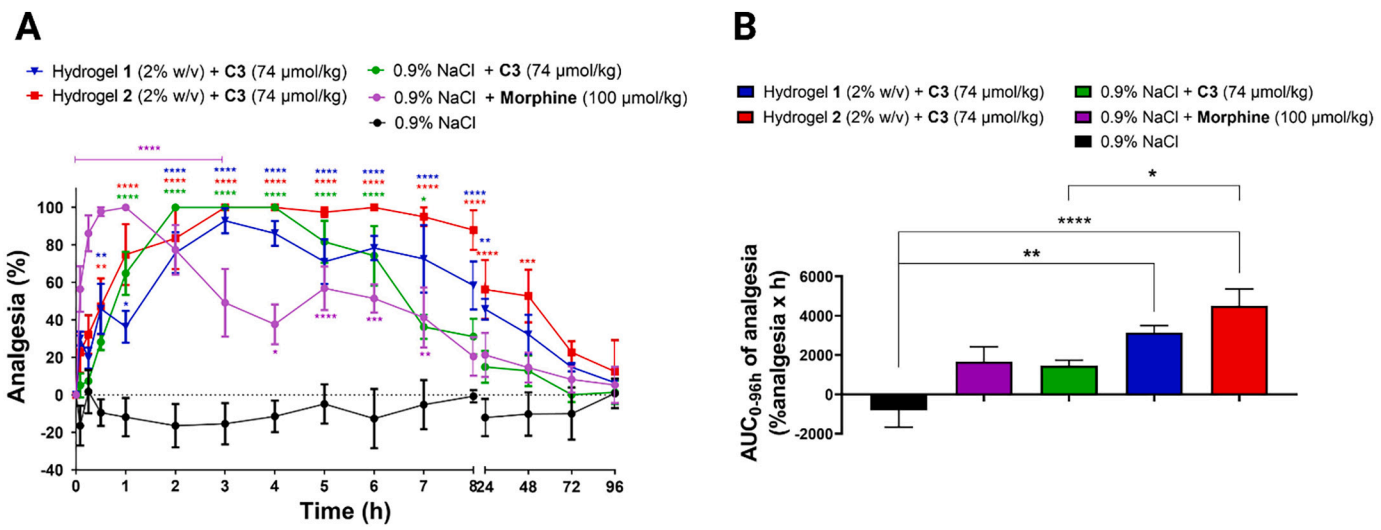

Fig. 7. Analysis of the antinociceptive activity of the analgesic peptide **C3** co-formulated with two different hydrogelators (**1** and **2**) and comparison to the activity of immediate release formulations (**C3** and morphine in 0.9% NaCl), using the *in vivo* hot-plate test after subcutaneous injection in mice. Groups of mice received either **C3** (74 μmol/kg) co-formulated with hydrogelators **1** and **2** (2% w/v gels in 0.9% NaCl), **C3** (74 μmol/kg) in 0.9% NaCl, morphine (100 μmol/kg) in 0.9% NaCl or 0.9% NaCl solution (control) (all administered in a volume of 5 μL/g). (A) Time course of the antinociceptive effects represented as % of analgesia after subcutaneous injection of the different formulations. Data points presenting mean values ± SD (n = 5): (*) $P < 0.05$, (**) $P < 0.01$, (***) $P < 0.001$, (****) $P < 0.0001$, comparison to T_0. (B) AUC values of the respective analgesia curves presenting as mean ± SD: (*) $P < 0.05$ hydrogel **2** + **C3** *vs.* 0.9% NaCl + **C3**, (**) $P < 0.01$ hydrogel **1** + **C3** *vs.* 0.9% NaCl, (****) $P < 0.0001$ hydrogel **2** + **C3** *vs.* 0.9% NaCl.

studied hydrogelators, at the same concentration, as determined *via* MTS assay (Fig. S14B). In addition to these *in vitro* biocompatibility data, body-weight changes and mice behaviour have been closely monitored as *in vivo* read-outs indicative of toxic effects. All animals in this study maintained a normal physical appearance, and no unusual behaviour or abnormalities were observed. As shown in Fig. S15, the hydrogelators showed negligible influence on the body-weight of the mice. Taken together, the subcutaneous administration of hydrogels, composed of hexapeptide **1** and dodecapeptide **2**, are thus believed to represent a safe path forward for the controlled-release of bioactive compounds.

4. Conclusion

In summary, we investigated the effect of doubling hydrogelator peptide length on fibre/network morphology, mechanical properties and sustained drug release behaviour of amphipathic peptide-based hydrogels. Specifically, doubling the hexapeptide lead sequence **1** (H-FQFQFK-NH_2) to thecorresponding dodecapeptide **2** (H-FQFQFKFQFQFK-NH_2) resulted in a more disordered fibrous network composed of shorter, slightly wider fibrils. The *in vitro* release studies point towards an influence of the cargo physicochemical properties on drug release behaviour, as cargoes **C1** and **C2** were only partly released from the gel network. However, the *in vitro* release profile of analgesic drug **C3** validated hydrogel **2** as controlled drug delivery platform. Most importantly and unique to this study is that *in vivo* properties of the two hydrogel systems have been investigated by non-invasive SPECT/CT imaging. This indicated an increased *in vivo* stability for hydrogel **2** compared to hydrogel **1**, which subsequently resulted in a more extended *in vivo* release of cargo **C2**. Hence, these results were validated for cargo **C3**, in view of future painkilling applications, showing the same promising effect for hydrogel **2**. Rheological measurements showed that the low mechanical properties of hydrogel **2** before injection could not be linked straightforwardly to the extended-release profiles. For the first time, post *in vivo* injection storage moduli were measured. The substantially increased values indicated a potentially important effect of the subcutaneous medium. Finally, the effectiveness of doubling the hydrogelator length was confirmed by a thermal nociceptive model (*i.e.* hot-plate test) after subcutaneous injection in mice, showing a more prolonged painkilling effect when comparing hydrogel **2** to hydrogel **1**. Altogether, increasing the hydrogelator length of amphipathic peptide-based hydrogels can be exploited as a useful strategy to alter hydrogel properties and optimize the targeted clinical effects.

CRediT authorship contribution statement

Julie Heremans: Investigation, Writing – original draft, Writing – review & editing. **Lucie Chevillard:** Investigation, Writing – review & editing. **Morgane Mannes:** Investigation, Writing – review & editing. **Jessica Mangialetto:** Investigation, Writing – review & editing. **Kaat Leroy:** Investigation, Writing – review & editing. **Jacinta F. White:** Investigation, Writing – review & editing. **Arthur Lamouroux:** Investigation, Writing – review & editing. **Mathieu Vinken:** Supervision, Writing – review & editing. **James Gardiner:** Investigation, Writing – review & editing. **Bruno Van Mele:** Supervision, Writing – original draft, Writing – review & editing. **Niko Van den Brande:** Supervision, Writing – original draft, Writing – review & editing. **Richard Hoogenboom:** Funding acquisition, Conceptualization, Writing – review & editing. **Annemieke Madder:** Funding acquisition, Conceptualization, Writing – review & editing. **Vicky Caveliers:** Funding acquisition, Conceptualization, Writing – review & editing. **Bruno Mégarbane:** Supervision, Writing – review & editing. **Sophie Hernot:** Supervision, Conceptualization, Writing – original draft, Writing – review & editing. **Steven Ballet:** Funding acquisition, Conceptualization, Writing – original draft, Writing – review & editing. **Charlotte Martin:** Supervision, Conceptualization, Writing – original draft, Writing – review & editing.

Declaration of Competing Interest

The authors declare no conflict of interest.

Acknowledgements

The Research Foundation Flanders is acknowledged for funding (G054119N, 1128520N). C.M., V.C., S.H. and S.B. thank the Research Council of the VUB for the financial support through the Strategic

Research Programme (SRP50). The authors thank TA Instruments for providing the Peltier Plate as well as Solvent Trap and Evaporation Blocker accessories.

Appendix A. Supplementary data

Description of the peptide synthesis and characterization. Additional *in vitro* characterization results (FT-IR spectroscopy, TEM images and rheometrical analyses). Additional *in vivo* imaging results and *in vitro/in vivo* biocompatibility data.

References

[1] J.-F. Jin, et al., The optimal choice of medication administration route regarding intravenous, intramuscular, and subcutaneous injection, Patient Prefer. Adherence 9 (2015) 923.
[2] M.E. Ruiz, S.S. Montoto, Routes of drug administration, in: ADME Processes in Pharmaceutical Sciences, Springer, 2018, pp. 97–133.
[3] D.N. McLennan, et al., Subcutaneous drug delivery and the role of the lymphatics, Drug Discov. Today Technol. 2 (1) (2005) 89–96.
[4] N. Gulati, H. Gupta, Parenteral drug delivery: a review, Recent Pat. Drug Deliv. Formul. 5 (2) (2011) 133–145.
[5] Y. Shi, L. Li, Current advances in sustained-release systems for parenteral drug delivery, Expert Opin. Drug Deliv. 2 (6) (2005) 1039–1058.
[6] D. Collins, et al., Optimizing the bioavailability of subcutaneously administered biotherapeutics through mechanochemical drivers, Pharm. Res. 34 (10) (2017) 2000–2011.
[7] W. Chen, et al., Improving long-term subcutaneous drug delivery by regulating material-bioenvironment interaction, Adv. Drug Deliv. Rev. 127 (2018) 20–34.
[8] B. Bittner, et al., Subcutaneous administration of biotherapeutics: an overview of current challenges and opportunities, BioDrugs 32 (5) (2018) 425–440.
[9] P. Muralidhar, E. Bhargav, Controlled release injectable drug delivery: an over view, Asian J. Biomater. Res. 3 (1) (2017) 6–15.
[10] A.A. Sheikh, S.R. Sheikh, Advanced injectable drug delivery system: a brief review, System 9 (2016) 11.
[11] K. Park, The controlled drug delivery systems: past forward and future back, J. Control. Release 190 (3) (2014) 3–8.
[12] T. Thambi, et al., Injectable hydrogels for sustained release of therapeutic agents, J. Control. Release 267 (2017) 57–66.
[13] G. Fichman, E. Gazit, Self-assembly of short peptides to form hydrogels: design of building blocks, physical properties and technological applications, Acta Biomater. 10 (4) (2014) 1671–1682.
[14] I.M. Geisler, J.P. Schneider, Evolution-based design of an injectable hydrogel, Adv. Funct. Mater. 22 (3) (2012) 529–537.
[15] M. Rivas, et al., Peptide self-assembly into hydrogels for biomedical applications related to hydroxyapatite, Gels 5 (1) (2019) 14.
[16] C. Martin, S. Ballet, Chapter 5 self-assembling hydrogels based on natural building blocks, in: Injectable Hydrogels for 3D Bioprinting, The Royal Society of Chemistry, 2021, pp. 112–140.
[17] Y. Li, et al., Peptide-based supramolecular hydrogels for delivery of biologics, Bioeng. Transl. Med. 1 (3) (2016) 306–322.
[18] W.Y. Seow, C.A. Hauser, Short to ultrashort peptide hydrogels for biomedical uses, Mater. Today 17 (8) (2014) 381–388.
[19] Z. Yu, et al., Engineering β-sheet peptide assemblies for biomedical applications, Biomater. Sci. 4 (3) (2016) 365–374.
[20] Charles J. Bowerman, B.L. Nilsson, Self-assembly of amphipathic b-sheets peptides: insights and applications, Biopolymers (Peptide Science) 98 (3) (2012).
[21] R.J. Betush, et al., Balancing hydrophobicity and sequence pattern to influence self-assembly of amphipathic peptides, Pept. Sci. 110 (1) (2018), e23099.
[22] C. Martin, et al., Injectable peptide-based hydrogel formulations for the extended in vivo release of opioids, Mater. Today Chem. 3 (2017) 49–59.
[23] M. Bibian, et al., Rational design of a hexapeptide hydrogelator for controlled-release drug delivery, J. Mater. Chem. B 3 (5) (2015) 759–765.
[24] E. Oyen, et al., In vivo imaging of the stability and sustained cargo release of an injectable amphipathic peptide-based hydrogel, Biomacromolecules 18 (3) (2017) 994–1001.
[25] C. Martin, et al., Biodegradable amphipathic peptide hydrogels as extended-release system for opioid peptides, J. Med. Chem. 61 (21) (2018) 9784–9789.
[26] N.R. Lee, et al., Sequence length determinants for self-assembly of amphipathic β-sheet peptides, Pept. Sci. 100 (6) (2013) 738–750.
[27] E.T. Pashuck, et al., Tuning supramolecular rigidity of peptide fibers through molecular structure, J. Am. Chem. Soc. 132 (17) (2010) 6041–6046.
[28] M.R. Caplan, et al., Control of self-assembling oligopeptide matrix formation through systematic variation of amino acid sequence, Biomaterials 23 (1) (2002) 219–227.
[29] M.B. Taraban, et al., Effects of chain length on oligopeptide hydrogelation, Soft Matter 7 (6) (2011) 2624–2631.
[30] M. Amblard, et al., Methods and protocols of modern solid phase peptide synthesis, Mol. Biotechnol. 33 (3) (2006) 239–254.
[31] N.B. Eddy, D. Leimbach, Synthetic analgesics. II. Dithienylbutenyl-and dithienylbutylamines, J. Pharmacol. Exp. Ther. 107 (3) (1953) 385–393.
[32] N.R. Lee, et al., Effects of varied sequence pattern on the self-assembly of amphipathic peptides, Biomacromolecules 14 (9) (2013) 3267–3277.
[33] C. Xavier, et al., 18F-nanobody for PET imaging of HER2 overexpressing tumors, Nucl. Med. Biol. 43 (4) (2016) 247–252.
[34] K. Van Holsbeeck, et al., Downsizing antibodies: towards complementarity-determining region (CDR)-based peptide mimetics, Bioorg. Chem. 119 (2022), 105563.
[35] M.A. Elsawy, et al., Controlling Doxorubicin Release from a Peptide Hydrogel through Fine-Tuning of Drug–Peptide Fiber Interactions, Biomacromolecules 23 (6) (2022) 2624–2634.